(Preprint) AAS 25-677

NETWORKS OF PERIODIC ORBITS IN THE EARTH–MOON SYSTEM THROUGH A REGULARIZED AND SYMPLECTIC LENS

Bhanu Kumar* and Agustin Moreno†

In this investigation, using numerical continuation, Kustaanheimo-Stiefel regularization, and a novel "symplectic toolkit", we carry out an extensive numerical study of periodic orbit families for the Earth–Moon CR3BP. Near the Moon we investigate prograde, retrograde, and Halo orbits, discovering previously-unknown orbit families linking them together through bifurcations and singularities – also confirming a 1968 conjecture of Broucke. Earth prograde and retrograde orbits are also studied, finding infinite chains linking $1{:}2N$ and $1{:}2N+1$ resonant orbits. These connections provide insights into the global network structure of families of periodic orbits, identifying orbit families near others of interest for mission design.

INTRODUCTION

The circular restricted 3-body problem (CR3BP) is a commonly used dynamical model for spacecraft motion in the Earth-Moon system. One class of CR3BP orbits which is critical for applications is periodic orbits (POs). Given their repeating and bounded nature, POs can provide useful operational orbits for spacecraft; for example, the well-known Halo orbits were used by the CNSA Chang'e 4 mission's Queqiao orbiter for lunar farside-to-Earth communications relay, and the future NASA-led Lunar Gateway also is planned to follow a near rectilinear halo orbit. Periodic orbits, particularly unstable ones, can also generate propellant-free pathways for spacecraft to follow through their stable & unstable manifolds. Thus, identifying and understanding the variety of POs in the Earth-Moon CR3BP is of significant importance for space operations in the region.

A number of previous studies - too many to comprehensively list here - have explored families of periodic orbits in the Earth-Moon CR3BP. Broucke[1] catalogued many different families of planar POs; later work, e.g. by Howell and Breakwell,[2] computed Halo orbits. Doedel et al[3] computed several families of POs emanating from the Earth-Moon libration points L1-L5 as well as analyzing their bifurcations, discovering geometric connections between several of the computed families. And recently, Russell and Franz[4] developed a database of millions of POs near the Moon using a grid search. However, gaps remain; for instance, Doedel et al[3] primarily considered bifurcations of libration point orbits. And while Russell and Franz[4] did not restrict to libration point orbits (restricting instead to the Moon's vicinity), they did not carry out any bifurcation analysis at all, thus leaving the question of how various PO families relate to each other unanswered.

In this paper, we aim to fill some of these gaps, carrying out a very thorough investigation of the bifurcation network structure of several Earth-Moon CR3BP periodic orbit families. This includes orbits both in the vicinity of the Moon, such as low and distant prograde, retrograde, and Halo orbits, as well as Earth-centered prograde, retrograde, and resonant periodic orbits. Our study discovers several previously-unknown families and connections between them by combining numerical continuation with two key additional tools: 1) regularization, and 2) a novel "symplectic toolkit". The former allows for periodic orbit continuations through singularities, revealing families previously thought of as disjoint to be in fact part of a smooth, unified whole – also confirming a conjecture made by R. Broucke[1] in 1968. The latter, developed by Moreno and collaborators,[5] leverages mathematical concepts from modern symplectic geometry, e.g. Conley-Zehnder (CZ) indices

*James Van Loo Postdoctoral Assistant Professor and NSF Postdoctoral Research Fellow, Department of Mathematics, University of Michigan, 530 Church St, Ann Arbor, MI 48109.
†Junior Professor, Institute for Mathematics, Heidelberg University, INF 205, 69120 Heidelberg, Germany.

and Floer numerical invariants – concepts hitherto unused in practical applications – to help characterize periodic orbits, detect their bifurcations, and find geometric relations between them.

After some background on the CR3BP and its regularization, this paper first presents a summary of the PO computation methods used in this study. An overview of the symplectic toolkit is then given, including a discussion of a new, easy-to-use, publicly available MATLAB tool we have released for computing orbit CZ indices. Next, the orbit families, bifurcations, and networks found are presented; while too many families are computed to demonstrate all of their orbits, the most relevant are discussed, and others are shown schematically on network diagrams. Finally, potential future applications, directions, & conclusions are discussed.

MODEL AND BACKGROUND

Circular Restricted 3-Body Problem

The circular restricted 3-body problem (CR3BP) models spacecraft motion under the gravitational influence of two large masses m_1 and m_2 which revolve about their barycenter in a circular Keplerian orbit (e.g. the Earth and Moon). Units are also normalized so that the distance between m_1 and m_2 becomes 1, their period of revolution 2π, and $\mathcal{G}(m_1+m_2)=1$. We define a mass ratio $\mu=\frac{m_2}{m_1+m_2}$ ($=1.215058\times10^{-2}$ for the Earth-Moon system), and use a synodic, rotating non-inertial Cartesian coordinate system centered at the m_1-m_2 barycenter with m_1 and m_2 always on the x-axis. Then, the equations of motion are

$$\ddot{x}=2\dot{y}+\frac{\partial U}{\partial x} \qquad \ddot{y}=-2\dot{x}+\frac{\partial U}{\partial y} \qquad \ddot{z}=\frac{\partial U}{\partial z} \tag{1}$$

$$U(x,y,z)=\frac{x^2+y^2}{2}+\frac{1-\mu}{r_1}+\frac{\mu}{r_2} \tag{2}$$

where $r_1=\sqrt{(x+\mu)^2+y^2}$ and $r_2=\sqrt{(x-1+\mu)^2+y^2}$ are the distances from the spacecraft to m_1 and m_2, respectively. Equation (1) can also be written in Hamiltonian form, with Hamiltonian given by

$$H(x,y,z,p_x,p_y,p_z)=\frac{(p_x+y)^2+(p_y-x)^2+p_z^2}{2}-U(x,y,z) \tag{3}$$

Hamilton's equations of motion due to Eq. (3) are equivalent to Eq. (1) under the substitutions $\dot{x}=p_x+y$, $\dot{y}=p_y-x$, and $\dot{z}=p_z$; we use the equations in terms of $(\dot{x},\dot{y},\dot{z})$ for computing periodic orbits, but the Hamiltonian form is required for computing CZ indices. The Hamiltonian in Eq. (3) is autonomous and thus is an integral of motion. $C=-2H$ is the *Jacobi constant*, and is often used in lieu of H to specify energy.

Symmetries The CR3BP has two symmetries which will be especially useful in this study to compute POs. In particular, given a CR3BP trajectory curve $\mathbf{x}(t)=(x(t),y(t),z(t))$, we have that:

1. the curve $\mathbf{x}_r(t)=(x(-t),-y(-t),z(-t))$ (reflected across the xz-plane) is also a solution.
2. the curve $\mathbf{x}_a(t)=(x(-t),-y(-t),-z(-t))$ (xz and xy-plane reflection) is also a solution.

Both symmetries require reversing the direction in which the curve is traversed with time, hence the evaluations of x,y, and z at $-t$. Note that the velocities along the symmetric trajectories are $\dot{\mathbf{x}}_r(t)=(-\dot{x}(-t),\dot{y}(-t),-\dot{z}(-t))$ for symmetry 1, and $\dot{\mathbf{x}}_a(t)=(-\dot{x}(-t),\dot{y}(-t),\dot{z}(-t))$ for symmetry 2.

The Kustaanheimo-Stiefel Regularization

The CR3BP equations of motion (1)-(2) have singularities at the positions of the two large masses, i.e. when $(x,y,z)=(1-\mu,0,0)$ and $(-\mu,0,0)$. At these points, Eqs. (1)-(2) are undefined for trajectory integration. Even away from but near these points, numerical integration of the standard CR3BP equations can become slow & inaccurate. *Regularization* addresses these issues by providing a coordinate transformation and rescaling of time under which the resulting equations of motion do not have a singularity at m_1 or m_2.

In this paper, we use the Kustaanheimo-Stiefel (KS) regularization[6] to remove the singularity at either $x = 1 - \mu$ *or* $-\mu$, depending on which body the orbits of interest pass near. While we refer the reader to Howell and Breakwell[2] for full details, we briefly discuss the transformation here and highlight a few key properties. Let S be the x-coordinate of the singularity to remove. The basic KS transform is then given by

$$\mathbf{R} = \begin{bmatrix} x - S \\ y \\ z \\ 0 \end{bmatrix} = \begin{bmatrix} u_1 & -u_2 & -u_3 & u_4 \\ u_2 & u_1 & -u_4 & -u_3 \\ u_3 & u_4 & u_1 & u_2 \\ u_4 & -u_3 & u_2 & -u_1 \end{bmatrix} \begin{bmatrix} u_1 \\ u_2 \\ u_3 \\ u_4 \end{bmatrix} = L(\mathbf{u})\mathbf{u} \tag{4}$$

Denoting $R = \|\mathbf{R}\|$, Equation (4) is accompanied by a time rescaling $dt = R\,ds$, where s is a "fictitious" time variable. As is described in Appendix A1 of Howell and Breakwell,[2] upon this transformation, the CR3BP differential equations relating $\frac{d^2\mathbf{u}}{ds^2}$ to $\mathbf{u}$ and $\frac{d\mathbf{u}}{ds}$ no longer have a singularity at $x = S$.

In this study, we will compute periodic orbits by finding their points on the plane $y = 0$. Note that if one takes $u_2 = u_4 = 0$, then Eq. (4) yields $y = 0$ automatically, along with $x - S = u_1^2 - u_3^2$ and $z = 2u_1u_3$. One can then transform any point $(x, 0, z)$ on the xz-plane to its KS vector $\mathbf{u} \in \mathbb{R}^4$ by the equation $u_1 + iu_3 = (x - S + iz)^{1/2}$ – either of the two complex square roots will work here. Thus, since it imposes no restrictions on x and z, we fix $u_2 = u_4 = 0$ when computing PO points lying on the xz-plane. Note that once $\mathbf{u}$ is found, one can compute $\frac{d\mathbf{u}}{ds} = \frac{1}{2}L(\mathbf{u})^T\frac{d\mathbf{R}}{dt}$, completing the full state transformation to KS variables; the selection $u_2 = u_4 = 0$ again imposes no restrictions on $\dot{x}$, $\dot{y}$, and $\dot{z}$ as $L(\mathbf{u})$ remains invertible.

COMPUTING CR3BP PERIODIC ORBITS

Due to the presence of an integral of motion, periodic orbits in the CR3BP occur in one-parameter families. Within these families, there may exist individual *critical* orbits from which new orbit families *bifurcate*, occurring when one of the non-trivial eigenvalues of the PO monodromy matrix passes through 1. Often, one has an orbit from some PO family, but needs to calculate other orbits in the same or a bifurcating family. For this, numerical continuation is necessary. We now summarize the methods used to compute POs in this study.

Symmetric Orbits

The previously-described symmetries of the CR3BP facilitate computation of periodic orbits as a result of the well-known mirror theorem.[7] Namely, if a trajectory passes through two phase-space points which remain unchanged by application of symmetry transformation 1 or 2, then this orbit must be periodic. For symmetry 1, such points are those that satisfy $(x, y, z, \dot{x}, \dot{y}, \dot{z}) = (x, -y, z, -\dot{x}, \dot{y}, -\dot{z})$, i.e. points with $y = \dot{x} = \dot{z} = 0$. For symmetry 2 one similarly requires $y = z = \dot{x} = 0$. Note that in either case, such points lie on the xz-plane $y = 0$. Orbits with symmetry 1 will be symmetric across the xz-plane, whereas those with symmetry 2 are symmetric about the x-axis; the latter we will henceforth refer to as axial symmetry.

To find such orbits, the goal is thus to compute initial phase space points $\mathbf{x} = (x_i, 0, z_i, 0, \dot{y}_i, 0)$ for xz-symmetry or $(x_i, 0, 0, 0, \dot{y}_i, \dot{z}_i)$ for axial symmetry such that after some number n of $y = 0$ Poincaré section mappings P, the resulting point $P^n(\mathbf{x}) = (x_f, 0, z_f, \dot{x}_f, \dot{y}_f, \dot{z}_f)$ also satisfies $\dot{x}_f = \dot{z}_f = 0$ or $z_f = \dot{x}_f = 0$; the required final condition $y_f = 0$ is guaranteed through use of the Poincaré map. We now describe how to compute such PO points, with and without regularization.

Physical coordinates In either symmetry case there are 3 unknown initial coordinates (denote them v_1, v_2, v_3) and 2 final conditions to be satisfied (denote them $w_1 = w_2 = 0$). Thus, the equations to be solved are underdetermined, as expected for 1-parameter families of solutions. Hence, for numerical continuation, we choose one of v_1, v_2, or v_3 as the continuation parameter, holding its value fixed while solving for the other two unknowns and changing the chosen parameter's value only at the next continuation step. This is essentially the method of Robin and Markellos[8] adapted to the $y = 0$ Poincaré map case, as described next.

With one of v_1, v_2, or v_3 fixed, we use a standard Newton method to solve for the other two. For this we need the derivatives $\frac{\partial w_i}{\partial v_j}$ for $i = 1, 2$ and j corresponding to the two unfixed coordinates. These partials will

be elements of the iterated Poincaré map's (matrix) derivative, which is given by

$$DP^n(\mathbf{x}) = \Phi(\tau, \mathbf{x}) - \dot{y}(P^n(\mathbf{x}))^{-1}\mathbf{f}(P^n(\mathbf{x}))[\Phi(\tau, \mathbf{x})_{row\,2}] \tag{5}$$

where $\mathbf{f}(P^n(\mathbf{x})) = [\dot{x}_f \;\; \dot{y}_f \;\; \dot{z}_f \;\; \ddot{x}_f \;\; \ddot{y}_f \;\; \ddot{z}_f]^T \in \mathbb{R}^6$ is the CR3BP flow vector given by the equations of motion Eq. (1)-(2) at the phase space point $P^n(\mathbf{x})$; τ is the time taken by $\mathbf{x}$ until its nth crossing $P^n(\mathbf{x})$ with the $y = 0$ plane under the flow; and $\Phi(\tau, \mathbf{x}) \in \mathbb{R}^{6\times 6}$ is the CR3BP state transition matrix at $\mathbf{x}$ for a time-τ propagation. The "row 2" subscript indicates that only the 1×6 second row vector from Φ is taken, so the second term in Equation (5) is the 6×6 matrix product of scalar $\dot{y}^{-1}$, a 6×1 column vector $\mathbf{f}$, and a 1×6 row vector $[\Phi(\tau, \mathbf{x})_{row\,2}]$. Thus, the RHS of Eq. (5) is valid.

With DP^n given by Equation (5), one can now extract the necessary partials. For instance, in the xz-symmetry case where u_1, u_2, u_3, w_1, and w_2 are $x_i, z_i, \dot{y}_i, \dot{x}_f$, and $\dot{z}_f$ respectively, the partials $\frac{\partial \dot{x}_f}{\partial x_i}$, $\frac{\partial \dot{x}_f}{\partial z_i}$, $\frac{\partial \dot{x}_f}{\partial \dot{y}_i}$, $\frac{\partial \dot{z}_f}{\partial x_i}$, $\frac{\partial \dot{z}_f}{\partial z_i}$ and $\frac{\partial \dot{z}_f}{\partial \dot{y}_i}$ are the (4,1), (4,3), (4,5), (6, 1), (6,3), and (6,5) row and column entries of DP^n, respectively. Four of these partials are used in the Newton method to converge a solution for the fixed continuation parameter, which is then changed slightly for the next step. Note that one can switch the parameter variable between steps, choosing any of v_1, v_2, or v_3 to increment.

With regularization As will be seen, periodic orbit families may pass through the collision singularities with m_1 or m_2. In such cases, we use a KS regularization[6] based method to continue periodic orbit families *through* the singularity at hand. Rather than solving for physical coordinates x_i, z_i, $\dot{y}_i$, and/or $\dot{z}_i$, we instead solve for KS-regularized initial state coordinates $\mathbf{U}_i = (u_{1i}, u_{2i}, u_{3i}, u_{4i}, u'_{1i}, u'_{2i}, u'_{3i}, u'_{4i})$ which yield the desired physical state through Eq. (4) and $\frac{d\mathbf{R}}{dt} = \frac{2}{R}L(\mathbf{u})\frac{d\mathbf{u}}{ds}$ (here $'$ signifies the fictitious-time derivative $\frac{d}{ds}$).

Our KS-based symmetric orbit continuation method is adapted from Howell and Breakwell,[2] who only considered xz-symmetry and did not use a $y = 0$ section. For the xz-symmetry case, we consider initial KS-states of form $\mathbf{U}_i = (u_{1i}, 0, u_{3i}, 0, 0, u'_{2i}, 0, u'_{4i})$, which ensures that the physical initial $\mathbf{x}$ satisfies $y_i = \dot{x}_i = \dot{z}_i = 0$, as required. For axial symmetry, though, we instead use initial KS-states of form $\mathbf{U}_i = (u_{1i}, 0, 0, 0, 0, u'_{2i}, u'_{3i}, u'_{4i})$ if $x_i > S$ in our orbit family or $\mathbf{U}_i = (0, 0, u_{3i}, 0, u'_{1i}, u'_{2i}, 0, u'_{4i})$ if $x_i < S$; this ensures the needed initial $y_i = z_i = \dot{z}_i = 0$. Denote the 4 unknown KS-state coordinates as v_1, v_2, v_3, v_4.

As in Howell and Breakwell, the orbit Jacobi constant will be used as the continuation parameter rather than any of the v_j. Thus, we need four scalar conditions (and their partials with respect to the v_j) to set up a Newton method to find $\mathbf{U}_i$. The Jacobi constant $C = C(x_i, y_i, z_i, \dot{x}_i, \dot{y}_i, \dot{z}_i)$ provides one such constraint, since the initial physical state $\mathbf{x} = (x_i, y_i, z_i, \dot{x}_i, \dot{y}_i, \dot{z}_i)$ is a function of $\mathbf{U}_i$. The partials $\frac{\partial C}{\partial v_j}$ can be extracted from $\nabla_{\mathbf{x}} C(\mathbf{x}(\mathbf{U}_i))\frac{d\mathbf{x}}{d\mathbf{U_i}}$, where $\nabla_{\mathbf{x}} C$ is a 1×6 gradient vector and $\frac{d\mathbf{x}}{d\mathbf{U_i}}$ is a 6×8 matrix. A second constraint with easy-to-find partials is given by requiring the time derivative of component 4 of Eq. (4) to be 0, i.e.

$$u_{4i}u'_{1i} - u_{3i}u'_{2i} + u_{2i}u'_{3i} - u_{1i}u'_{4i} = 0 \tag{6}$$

For the remaining two needed scalar constraints, these are given by the fact that with $\mathbf{x} = \mathbf{x}(\mathbf{U}_i)$, the final point $P^n(\mathbf{x})$ under the $y = 0$ Poincaré map P must satisfy $R\dot{x}_f = R\dot{z}_f = 0$ for xz-symmetry or $z_f = R\dot{x}_f = 0$ for axial symmetry. Denote the appropriate two final conditions as $w_1 = w_2 = 0$. Then, to find $\frac{\partial w_k}{\partial v_j}$ for $k = 1, 2$ and $j = 1, 2, 3, 4$, the first step is to compute the derivative of P^n *expressed in KS-coordinates*. Namely, let P_{ks} be the Poincaré map in KS-state space $\mathbf{U} \in \mathbb{R}^8$ for the section $y(\mathbf{U}) = 2u_1u_2 - 2u_3u_4 = 0$, propagating points by the KS-regularized CR3BP equations of motion until their first return to this section. Then, denoting $\mathbf{U}_f = P^n_{ks}(\mathbf{U}_i) = (u_{1f}, u_{2f}, u_{3f}, u_{4f}, u'_{1f}, u'_{2f}, u'_{3f}, u'_{4f})$, we have

$$DP^n_{ks}(\mathbf{U}_i) = \Phi_{ks}(\tau_s, \mathbf{U}_i) - \mathbf{f}_{ks}(\mathbf{U}_f)\frac{\nabla y(\mathbf{U}_f)\Phi_{ks}(\tau_s, \mathbf{U}_i)}{\nabla y(\mathbf{U}_f)\mathbf{f}_{ks}(\mathbf{U}_f)} \tag{7}$$

where $\mathbf{f}_{ks}(\mathbf{U}_f) \in \mathbb{R}^8$ is the KS-regularized CR3BP flow vector at $\mathbf{U}_f$; τ_s is the fictitious KS-time taken by $\mathbf{U}_i$ until its nth crossing $\mathbf{U}_f$ with the $y = 0$ section under the KS flow; and $\Phi_{ks}(\tau_s, \mathbf{U}_i) \in \mathbb{R}^{8\times 8}$ is the KS-regularized CR3BP flow's state transition matrix at $\mathbf{U}_i$ for a fictitious KS time-τ_s propagation. Note that $\nabla y(\mathbf{U}_f) = [2u_{2f} \;\; 2u_{1f} \;\; -2u_{4f} \;\; -2u_{3f} \;\; 0 \;\; 0 \;\; 0 \;\; 0]$ is a 1×8 vector, so the denominator in Eq. (7) is a scalar.

We can now find the derivatives $\frac{dw_k}{d\mathbf{U}_i} = \nabla w_k(\mathbf{U}_f) DP^n_{ks}(\mathbf{U}_i)$, $k = 1, 2$. For $w_k = R\dot{x}_f$ or $R\dot{z}_f$, $\nabla w_k(\mathbf{U}_f)$ can be found as the gradient (with respect to the 8D KS-state) of component 1 or 3 of $2L(\mathbf{u})\mathbf{u}'$, evaluated at $\mathbf{U}_f$. For $w_k = z_f$, $\nabla w_k(\mathbf{U}_f)$ is similarly found as the gradient of component 3 of Eq. (4). From the derivatives $\frac{dw_k}{d\mathbf{U}_i}$, the partials $\frac{\partial w_k}{\partial v_j}$ with respect to our unknowns v_j can finally be extracted. Along with the Jacobi constant condition and Eq. (6), this completes the 4×4 matrix of partials required to solve for $\mathbf{U}_i$ by Newton's method. As mentioned earlier, the solution $\mathbf{U}_i$ yields the desired initial Cartesian state $\mathbf{x}$ as well. Finally, once $\mathbf{U}_i$ is found at the desired Jacobi constant, C is changed slightly for the next continuation step.

Non-Symmetric Orbits

While most of the orbits in this study have either xz-plane or axial symmetry, we also compute a few PO families not satisfying either symmetry. To compute such orbits, we will seek points $\mathbf{x} = (x_i, 0, z_i, \dot{x}_i, \dot{y}_i, \dot{z}_i)$ such that $P^n(\mathbf{x}) = \mathbf{x}$ for some $n \in \mathbb{Z}$; we assume n is known beforehand, since the asymmetric orbits we study will bifurcate from previously-computed symmetric orbits. Computation methods for such orbits, both with and without regularization, are described next.

Physical coordinates At first glance, it may seem that to solve $P^n(\mathbf{x}) = \mathbf{x}$ for the five unknown coordinates of $\mathbf{x}$, one will set up a 5×5 derivative for the Newton correction step. However, recall that the CR3BP has an integral of motion: the Jacobi constant C. Thus, if the equation $P^n(\mathbf{x}) = \mathbf{x}$ is satisfied in four of the five components $x, z, \dot{x}, \dot{y}$, and $\dot{z}$ (in addition to being trivially satisfied in its y component due to the use of a $y = 0$ Poincaré section), then one will have that the equation is in fact also automatically satisfied in all six state components. Thus, in reality one only needs to satisfy 4 scalar constraint equations, rather than 5; once again we have more unknowns than constraints.

To set up an equation in 4 unknowns and constraints, similar to the symmetric case, one of the 5 unknowns x_i, z_i, $\dot{x}_i, \dot{y}_i$, and $\dot{z}_i$ is chosen as the continuation parameter and fixed. Denote the 4 non-fixed unknowns as v_1, v_2, v_3, and v_4. Then, denoting $P^n(\mathbf{x}) = (x_f, 0, z_f, \dot{x}_f, \dot{y}_f, \dot{z}_f)$ as before, we solve the four scalar equations $x_f(\mathbf{x}) - x_i = 0$, $z_f(\mathbf{x}) - z_i = 0$, $\dot{x}_f(\mathbf{x}) - \dot{x}_i = 0$, and $\dot{y}_f(\mathbf{x}) - \dot{y}_i = 0$ for the v_j. To set up Newton's method for these equations, as in the symmetric case, the 16 required partials $\frac{\partial x_f}{\partial v_j}$, $\frac{\partial z_f}{\partial v_j}$, $\frac{\partial \dot{x}_f}{\partial v_j}$, and $\frac{\partial \dot{y}_f}{\partial v_j}$, $j = 1, 2, 3, 4$ can be extracted from the matrix $DP^n(\mathbf{x})$ given by Eq. (5). Once a solution is converged, the continuation parameter is changed slightly and the process repeated; one can also switch to a different parameter between continuation steps, choosing any of $x_i, z_i, \dot{x}_i, \dot{y}_i$, and $\dot{z}_i$ to increment in the next step.

With regularization In this paper, we only compute planar asymmetric orbits, so our KS-based asymmetric orbit continuation method only works with planar orbits for now. As in the symmetric case, we solve for KS-regularized initial states rather than physical coordinates; however, for planar asymmetric orbits, we will consider initial KS-states of form $\mathbf{U}_i = (u_{1i}, 0, 0, 0, u'_{1i}, u'_{2i}, 0, 0)$ if $x_i > S$ in the family being studied or $\mathbf{U}_i = (0, 0, u_{3i}, 0, 0, 0, u'_{3i}, u'_{4i})$ if $x_i < S$. Such states ensure $y_i = z_i = \dot{z}_i = 0$ (planar orbit point on $y = 0$ section) as well as automatically satisfying condition Eq. (6). As in the symmetric case, we continue orbits by Jacobi constant, so we will have 3 unknown KS coordinates to solve; denote them v_1, v_2, and v_3.

Now, we need 3 scalar conditions to solve for our three unknowns. One condition will again be given by the fixed Jacobi constant C during each continuation step; its partials are computed exactly as in the symmetric orbit case. The other two conditions will be from expressing the x and $\dot{y}$ components of $P^n(\mathbf{x}) - \mathbf{x} = 0$ as functions of $\mathbf{U}_i$. Denote the transformations from KS states $\mathbf{U} \in \mathbb{R}^8$ to Cartesian scalar coordinates x, $\dot{y}$ as $x(\mathbf{U}), \dot{y}(\mathbf{U}) : \mathbb{R}^8 \to \mathbb{R}$, and recall the KS-coordinate $y(\mathbf{U}) = 0$ Poincaré map P^n_{ks} defined earlier in the symmetric orbits section. Then, we want

$$x(P^n_{ks}(\mathbf{U}_i)) - x(\mathbf{U}_i) = 0 \qquad \dot{y}(P^n_{ks}(\mathbf{U}_i)) - \dot{y}(\mathbf{U}_i) = 0 \tag{8}$$

The derivative DP^n_{ks} with respect to initial $\mathbf{U}_i$ was given by Eq. (7); the derivatives $\frac{dx}{d\mathbf{U}}$ and $\frac{d\dot{y}}{d\mathbf{U}}$ at $\mathbf{U}_f = P^n_{ks}(\mathbf{U}_i)$ and $\mathbf{U}_i$ are found by differentiating component 1 of Eq. (4) and component 2 of $\frac{2}{R}L(\mathbf{u})\mathbf{u}'$ respectively, and evaluating at $\mathbf{U}_f$ and $\mathbf{U}_i$. These derivatives allow us to find the $\mathbf{U}_i$-derivatives of the LHS of both conditions in Eq. (8), from which the partials with respect to v_1, v_2, and v_3 can be extracted. Combining with the constraint on C, we get a 3×3 matrix of partials to solve $\mathbf{U}_i$ by Newton's method, also yielding $\mathbf{x}$. The value of C is then changed for the next continuation step and the process repeated, as in the symmetric case.

Some Notes on Continuation and Bifurcation Analysis

In the previously-described methods, one continues periodic orbits either by stepping in some initial state coordinate $x_i, z_i, \dot{x}_i, \dot{y}_i, \dot{z}_i$, or by stepping in Jacobi constant C. At times, the chosen continuation parameter might reach an extremum along the PO family, past which no family orbits exist; further continuation in that parameter will then fail. In such cases, changing the continuation parameter to a different variable or to C is useful. We have yet to find an orbit family where such a change of parameter did not allow us to proceed.

Once periodic orbits in a family are computed, their 6×6 monodromy matrices and those matrices' eigenvalues can be found. Since the CR3BP is Hamiltonian, all PO monodromy matrices will have a double eigenvalue of 1; the other four eigenvalues will occur as two (possibly complex) reciprocal pairs and are called the *Floquet multipliers*. In the important special case of planar symmetric orbits (with $z = \dot{x} = \dot{z} = 0$ at the symmetric intersection point with the $y = 0$ section), orbits in such families will have monodromy matrices which can be decomposed[9] into 4×4 planar and 2×2 spatial blocks, with one planar and one spatial pair of Floquet multipliers.

Generally, both Floquet multiplier pairs will be away from 1, but it can happen that at some isolated orbits in the family, a pair of Floquet multipliers passes through 1. Such an orbit is called a *critical orbit*, and generates a *bifurcation*. At any such bifurcation, one of two things occurs: 1) the Jacobi constant takes an extremum (called a *fold bifurcation*), or 2) the Jacobi constant does not take an extremum, and at least one other orbit family emerges from the critical orbit, distinct from the original orbit family. To find the new orbits which occur in the non-fold case, one should find the unit eigenvectors of the monodromy matrix. One such eigenvector will occur in the flow direction and can be ignored, but any others will indicate directions in which bifurcating orbit families lie.

In this paper, we will study various bifurcations of planar symmetric orbits. In the case of such an orbit's planar Floquet multipliers going through 1, this can indicate either a fold bifurcation or a symmetry-breaking planar bifurcation where the corresponding unit eigenvector has a nonzero $\dot{x}$ component; in this case, the bifurcating orbit family can be found by starting an asymmetric orbit continuation by $\dot{x}$ from the symmetric critical orbit. In the case of a planar symmetric orbit's spatial Floquet multiplier going through 1 instead, one expects spatial periodic orbits to emerge. The symmetry of any bifurcating spatial orbits is determined by the monodromy matrix unit eigenvector(s); if the eigenvector has component $z \neq 0, \dot{z} = 0$, the orbits have xz-symmetry and can be found by symmetric continuation in z, whereas an eigenvector with $\dot{z} \neq 0$, $z = 0$ implies axial symmetry (its orbits can be computed by continuation in $\dot{z}$). If two unit eigenvectors exist spanning the entire $(z, \dot{z})$ space, then two spatial orbit families emerge, one each for xz- and axial symmetry.

THE SYMPLECTIC TOOLKIT

While the previously described methods allow computation of periodic orbit families, including those emerging from bifurcations, the bifurcation analysis requires keeping track of various Floquet multipliers and their corresponding monodromy matrix eigenvectors. Furthermore, studying the potential connectedness of already-known periodic orbit families involves fully continuing them first and then comparing orbits between families, requiring sifting through a great deal of information. Recently, a "symplectic toolkit" has been developed[5] that helps simplify such analyses, by leveraging the concepts of Conley-Zehnder (CZ) indices and Floer numerical invariants from the mathematical field of symplectic geometry to help detect periodic orbit bifurcations and find connections between them. This toolkit consists of four main tools; they are:

1. **The B-signs**:[10] a $\pm$ sign associated to each elliptic or hyperbolic Floquet multiplier of an orbit, which helps predict bifurcations. This generalizes the classical Moser–Krein signature – which applies only to elliptic Floquet multipliers – to also include the case of hyperbolic multipliers for *symmetric* orbits.

2. **Global topological methods:** the *GIT-sequence*[10] of spaces whose global topology encodes (and at times forces) bifurcations. It refines Broucke's stability diagram[11] by adding B-signs.

3. **Conley-Zehnder (CZ) index:**[12,13] an integer winding number associated to each non-critical orbit, extracted from the topology of the symplectic matrix group. It does not change unless a bifurcation

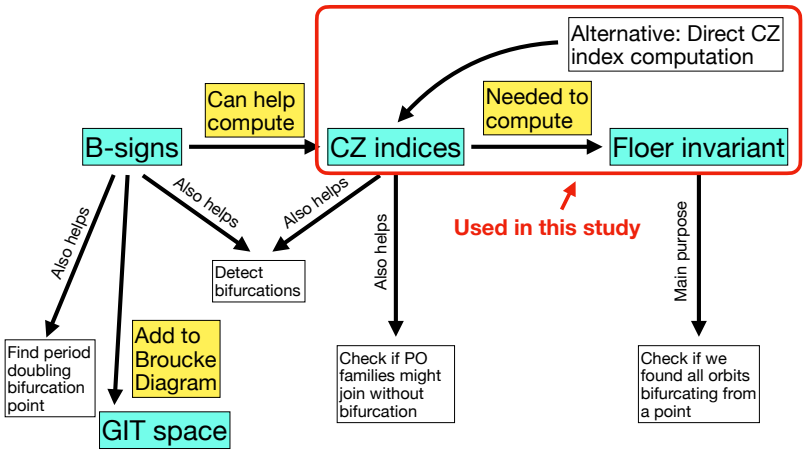

Figure 1: Summary of the symplectic toolkit, with the tools used in this study indicated

occurs. Therefore it can be used to determine which families connect to which.

4. **Floer invariant (or Floer number):** Numbers which stay invariant before and after a bifurcation, and so can help predict the existence of orbits, as well as being easy to implement. There is one invariant for arbitrary periodic orbits, and another for *symmetric* periodic orbits.[5] It is

$$\chi(x) = \sum_{i \in before} (-1)^{CZ_i} = \sum_{j \in after} (-1)^{CZ_j} \tag{9}$$

where the first and second sums are over orbits before and after bifurcation, respectively.

The utility of and relationships between the different tools are summarized in Fig. 1. In this study, we use the CZ index and Floer invariant to assist in our analyses. Changes of CZ-index indicate bifurcations. And at bifurcations, the Floer invariant helps verify that all emerging orbits have been found – if the sum of Eq. (9) does not match over all orbits found before and after the bifurcation, some orbit must remain to be found.

Conley-Zehnder Index Calculator

For this study, based on a similar Python code due to Otto van Koert*, a CZ-index calculator was developed in MATLAB by implementing the method described in Moreno et al.[9] The program is extremely simple to use and suitable for practitioners, requiring no knowledge of theory. It provides two CZ index functions, one for any orbit and one for planar orbits, with the following syntax:

```
[cz_idx] = get_cz_index(state, period, mu, steps, error_report)
[cz_idx, cz_pl, cz_sp] = get_split_cz_index(state, period, mu)
```

These MATLAB codes are available publicly at `https://github.com/bhanukumar314`.

Both functions take as inputs the periodic orbit's 6D initial state vector `state`, the orbit `period`, and the CR3BP mass ratio `mu` being used. The `get_cz_index` function can be used for any periodic orbit, and outputs the orbit CZ index. It has two optional arguments: `steps` and `error_report`. The former controls the number of discretization steps used to construct a required path from the orbit's monodromy matrix to certain special "base matrices", as detailed in Moreno et al;[9] if true, `error_report` simply displays a number of values which give information about the computation's accuracy. Arguments `steps` and `error_report` have default values of 20000 and `false`.

The `get_split_cz_index` function on the other hand only works for planar POs lying in the $z = 0$ plane for all time, but it provides more information while requiring less computation. It does not require

*Available at `https://github.com/ovkoert/cz-index`

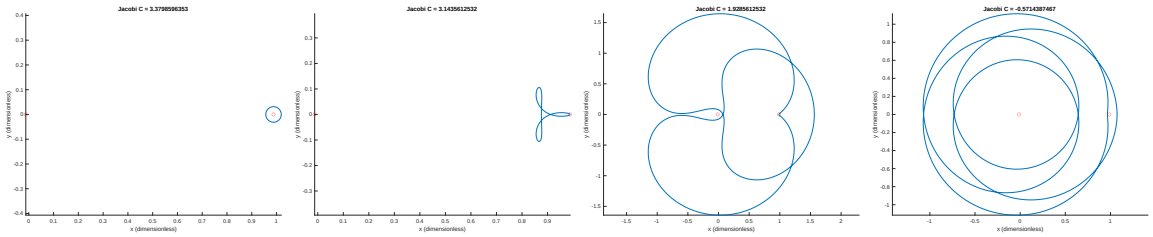

Figure 2: A few selected orbits from Broucke's H1 family, decreasing Jacobi constant

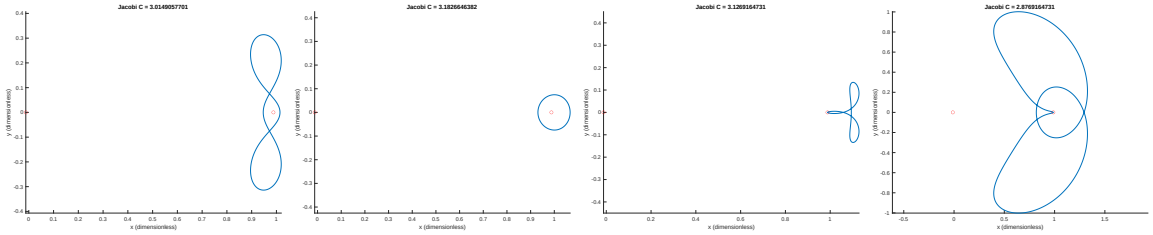

Figure 3: A few selected orbits from Broucke's H2 family, DPO to near-circular to LPO

constructing any matrix path to any base matrix, hence the absence of optional arguments `steps` and `error_report`. Furthermore, it calculates not only the orbit's total CZ index `cz_idx`, but also its *planar* and *spatial* CZ indices `cz_pl` and `cz_sp`, respectively. This helps determine whether a given planar orbit's bifurcation will lead to another planar orbit, or to a spatial one. One has `cz_idx = cz_pl + cz_sp`; this total CZ index given by `get_split_cz_index` will match that from `get_cz_index` for any planar orbit.

With this program, applying the symplectic toolkit for bifurcation analysis becomes very easy. With one line of code, the CZ indices for any periodic orbit can be computed. Finding these indices for different periodic orbits, Floer invariants can then be computed before and after bifurcations, allowing us to verify whether or not all emerging orbits have been computed as described earlier.

RESULTS: ORBIT FAMILIES AND NETWORKS

Using the periodic orbit continuation methods described earlier and the symplectic tools just described, we carried out a thorough study of four different PO families and their bifurcations in the Earth-Moon CR3BP. These families are the ones that start as small 1) prograde circles around the Moon, 2) prograde circles around the Earth, 3) retrograde circles around the Moon, and 4) retrograde circles around the Earth. These four families are planar and symmetric; many of their orbits were computed by R. Broucke in his 1968 JPL report,[1] but even just continuing these families further using our KS regularization-based methods yields surprising new results. Then, carrying out a bifurcation analysis of these families yields even more orbits, also revealing previously unknown connections between various orbit types. We present all these results next.

Remark Unless otherwise specified, we will only study bifurcations occurring when an orbit Floquet multiplier pair passes through 1. We do not study period-doubling (where the Floquet pair passes through -1), nor any other n-fold bifurcations due to Floquet multipliers passing through nth roots of unity with $n > 1$.

Lunar Prograde Orbits, Broucke's Conjecture, and Bifurcations Connecting to Halo Orbits

Prograde planar symmetric orbits around the Moon were studied by Broucke,[1] who found two such PO families that he labeled H1 and H2. These families, a few of whose orbits are shown in Figures 2-3, include what are called the low prograde & distant prograde lunar orbits (LPOs/DPOs). H1 begins with small circular lunar orbits, which become LPOs that "stretch" towards the L1 libration point, then followed by other types of orbits. H2 starts with highly eccentric DPOs that then become nearly circular, subsequently morphing into LPOs stretching towards L2. On page 71 of his report, Broucke conjectures "It is likely that, if one were to continue family H1 or the two open ends of H2, some junction between H1 and H2 would be found."

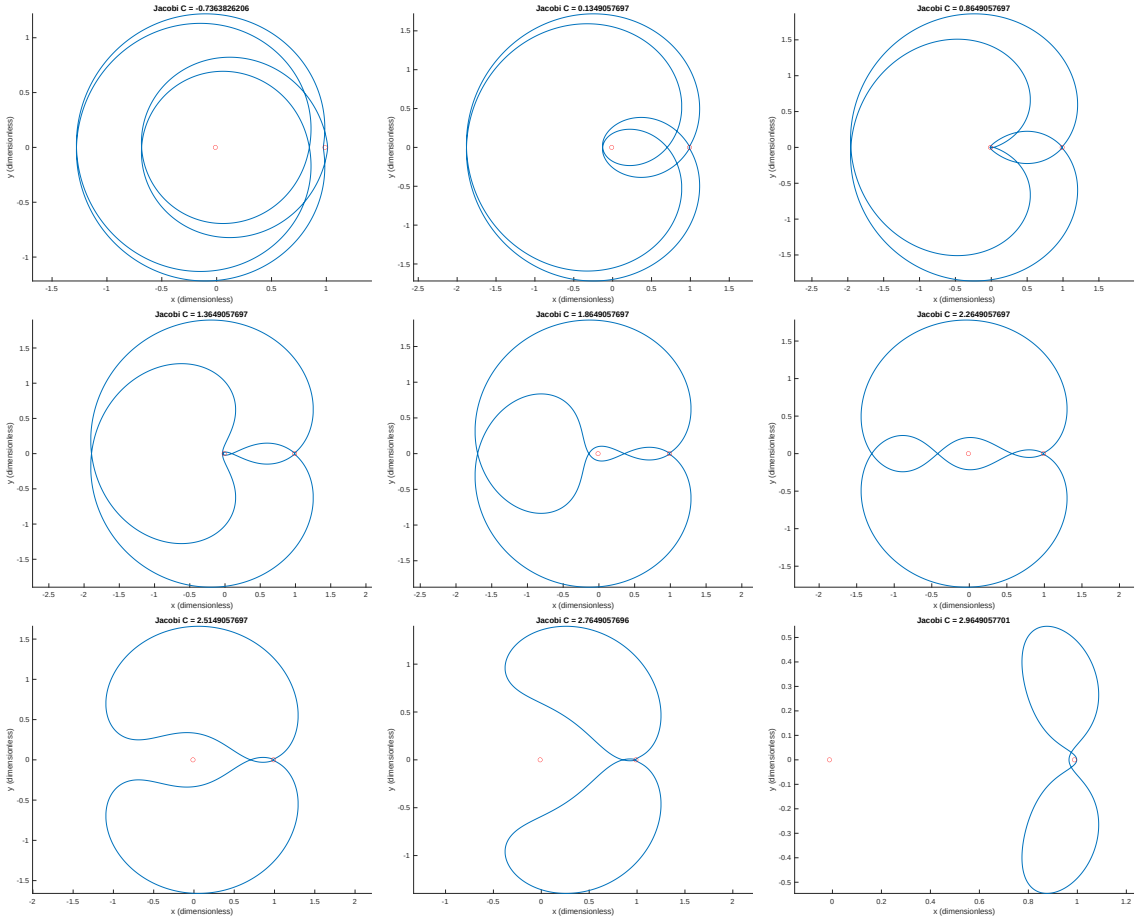

Figure 4: Orbit family joining H1 to H2, $C = -0.736$ to 2.965 (going right, then down). The top left orbit is among the last in H1; the bottom right orbit begins H2. Red circles at positions of Earth and Moon.

Using our KS-regularized symmetric orbit continuation method, 57 years later, we have discovered Broucke's conjectured junction – thus showing that H1 and H2 in fact belong to a single PO family. Figure 4 displays a selection from the series of orbits that connect Broucke's final H1 orbit (no. 162) to Broucke's H2 orbit no. 1 (a DPO). The orbit family passes once through the Earth singularity and then through the Moon singularity. To our knowledge, such an H1 to H2 link has never been shown before; Lara and Russell[14] found spatial families of orbits linking double-period covers of H1 and H2, but their orbits are not in the $z = 0$ plane and cannot be considered as part of the H1 or H2 families. In contrast, our orbits joining H1 and H2 are planar and symmetric like H1 and H2, and do belong to the same continuous orbit family as H1 and H2.

We also tried further continuing Broucke's final H2 orbit (no. 202) to see if the unified family reaches any natural termination point, but none was found even after significant further continuation. Thus, we next turned our attention to study bifurcations of this orbit family. A bifurcation diagram of the unified H1-H2 family is shown in Figure 5, with critical orbit Jacobi constants labeled (note that C decreases as one moves up the diagram). The CZ indices of unified family orbits and of the first few orbits in each bifurcating family are also displayed. It can be verified that the Floer invariant matches before and after every bifurcation; for example, for the bifurcation at $C = 3.136$, the Floer number is $(-1)^6 = 1$ for $C > 3.136$, and $(-1)^6 + (-1)^7 + (-1)^6 = 1$ for $C < 3.136$.

The bifurcation analysis shown in Figure 5 is comprehensive for single covers* of this unified H1-H2 family; it accounts for all bifurcations up to the fold bifurcation at $C = -1.282$, which corresponds to one of the

*i.e. not counting period-doubling or other n-fold bifurcations for $n > 1$, as mentioned in the remark earlier

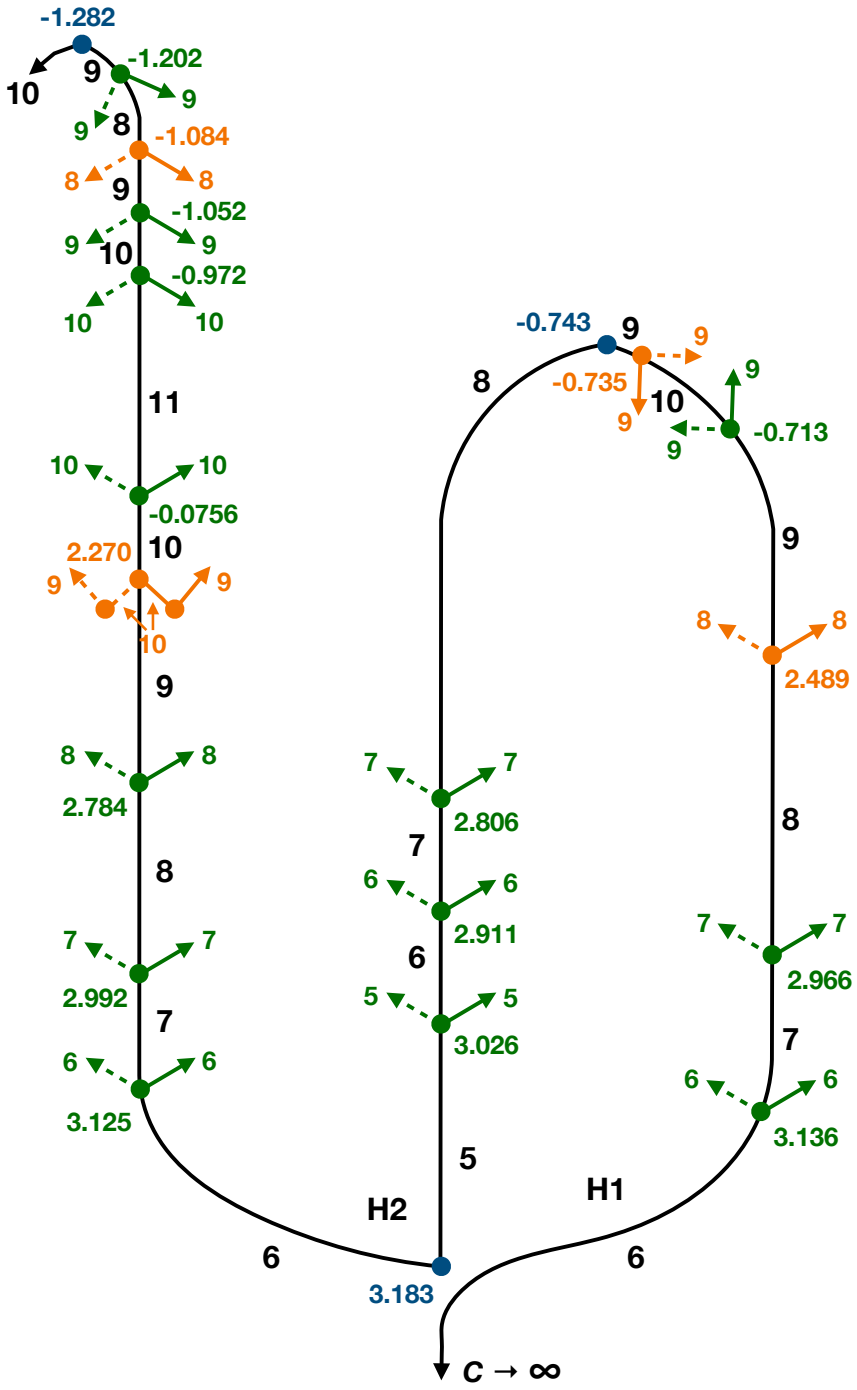

Figure 5: A bifurcation diagram for the unified H1-H2 prograde orbit family. Green dots indicate out-of-plane bifurcations, orange represent planar symmetry-breaking bifurcations, and dark blue are fold bifurcations. Decimal numbers are Jacobi constants C of critical (bifurcation) orbits; C decreases (energy increases) as one moves up the page. The integers are CZ indices. Dotted lines indicate that the corresponding families have been obtained by reflection along the xy-plane (for spatial orbits) or xz-plane (for planar asymmetric orbits) of the families represented by solid lines.

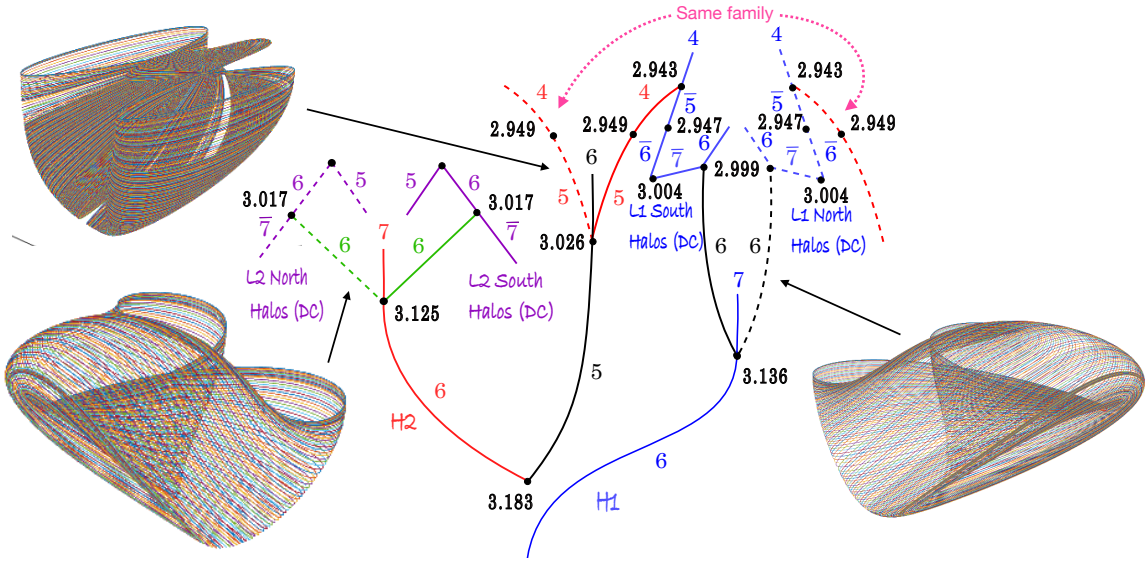

Figure 6: Bifurcation graph relating H1 & H2 orbits with L1 & L2 Halo double cover orbits, with CZ indices & bifurcation C values labeled. Orbits from the 3 new families are also shown, with arrows indicating the corresponding graph edges. Dotted lines indicate orbits obtained by reflection. Bars over CZ indices indicate that the corresponding orbits are *homologically-bad* (do not affect the Floer invariant). The two dotted red curves represent the same family and should be identified.

last orbits found from continuing H2 past Broucke's final H2 orbit. The green curves and values correspond to spatial orbit bifurcations, while orange represents planar symmetric-to-asymmetric bifurcations. In either case, the CR3BP's symmetries mean that two new orbit families emerge: either a pair of spatial families which are xy-plane reflections of each other (in the spatial bifurcation case) or a pair of planar families which are xz-plane reflections (in the symmetry-breaking planar case). While far too many bifurcating families were computed to present all of them in this paper, we highlight details of a few interesting ones next.

Out-of-plane bifurcations Changes of spatial CZ indices alerted us to planar-to-spatial orbit bifurcations, which were also confirmed by computing Floquet multipliers. 13 such bifurcations were found, shown in green in Figure 5. Of these, the bifurcations at $C = 3.136, 3.026$, and 3.125 – corresponding to critical H1 LPO, H2 DPO, and H2 LPO orbits respectively – generate orbit families linking H1 and H2 to the well-known Halo orbits. And the bifurcation at $C = 2.992$, a critical H2 LPO, generates a spatial orbit family which then returns to the H2 family, to the critical H2 DPO at $C = 2.911$. It is these bifurcations we will focus on here.

The bifurcating orbits at $C = 3.136, 3.026$, and 3.125 are summarized in the bifurcation network diagram of Figure 6. We found three new xz-symmetric orbit family pairs emerging from H1 LPO, H2 LPO, and H2 DPO orbits and connecting them respectively to L1, L2, and L1 (Northern & Southern) Halo orbit double covers. By double cover (or nth cover more generally) of a periodic orbit, we refer to the periodic orbit generated by traversing the original PO twice (or n times); the families emerging from H1 and H2 in Figure 6 thus end at period-doubling bifurcations of Halo orbits. The Floer invariant can be verified to match before and after each bifurcation in Fig. 6, except the one between the red CZ 4 and 5 segments. Thus, except that one case, we have strong evidence that no further orbit families emerge from the shown bifurcations.

Similar families connecting LPOs to Halos and DPOs to vertical collisions were discovered in the Hill restricted 3-body problem (HR3BP) by Aydin and Batkhin,[15] whose results served as an impetus to search for similar CR3BP orbits; in the CR3BP, Halo orbits take the place of HR3BP vertical collision orbits. While a few of our Earth-Moon H2-to-L2-Halo orbits were computed by Howell and Campbell[16] starting from the period-doubling bifurcation of L2 Halos, the connection to the planar H2 family was not discovered by them. And though a few of our H2 DPO to L1 Halo orbits were found by Franz and Russell,[4] they did not compute the full family nor uncover its connections to Halo and DPO families; this family passes through the singularity at the Moon and required KS regularization to compute, which was not carried out in their study.

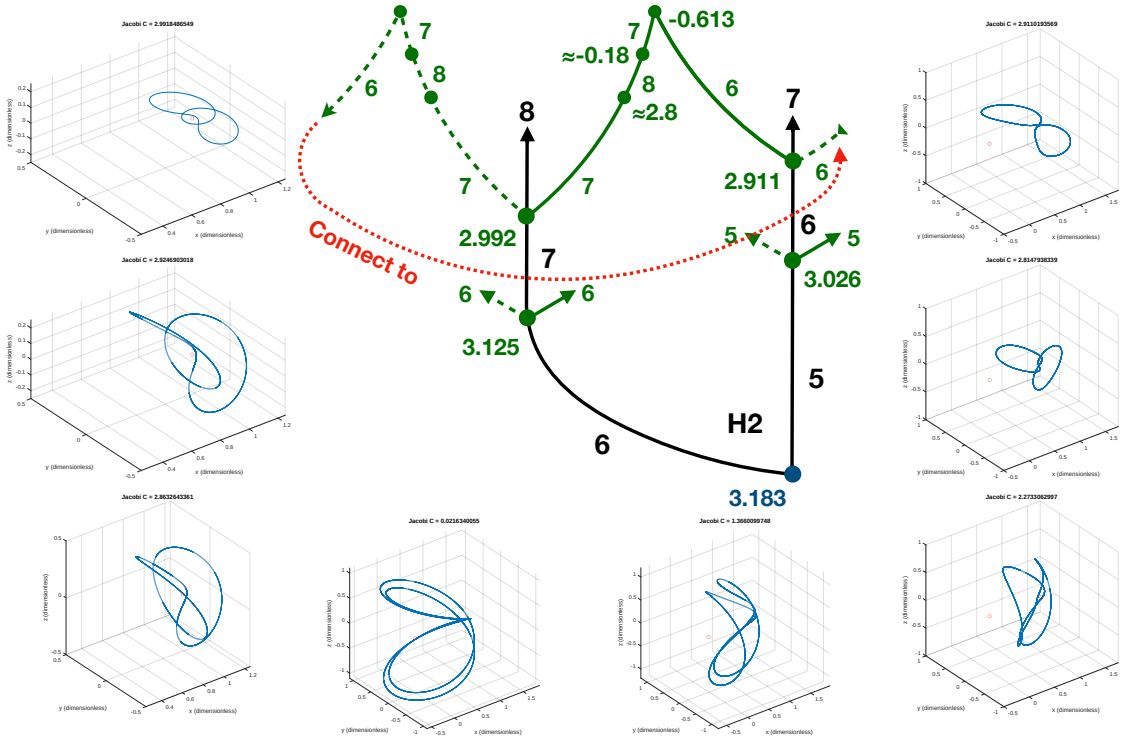

Figure 7: Bifurcation graph and orbits for H2 LPO to H2 DPO family with CZ indices & bifurcation C values labeled. Green dotted lines indicate family obtained by reflection. Orbits are shown in the same order they are encountered as one moves along the family, starting with the critical LPO (top left plot), then moving down the plots, then right, then up, ending at the critical DPO (top right plot).

Another interesting out-of-plane bifurcation from the H2 orbits is an orbit family pair emerging from the H2 LPO at $C = 2.992$ and ending at an H2 DPO at $C = 2.911$. The diagram of Figure 7 displays the relationship of this family to those of Figure 5. This "LPO-DPO bridge" family itself has a fold bifurcation at $C = -0.613$ and other bifurcations at $C \approx -0.18$ and 2.8, as shown in the figure; more families should emerge from the $C \approx -0.18$ and 2.8 critical orbits, though we did not compute them or investigate these bifurcations beyond noting CZ index changes and approximate critical orbit C values. The evolution of orbits in this LPO-DPO bridge family is also displayed in Figure 7. All orbits in this family have axial symmetry.

The spatial families thus far discussed account for 5 of the 13 spatial bifurcations shown in Figure 5. The remaining bifurcating spatial orbit families mostly did not display any connections to other known orbits; the families emerging at $C = 2.784$, -0.0756, and -1.052 terminate at planar symmetric orbits of unknown type. The family pair emerging from $C = -1.202$ passes through (but does not end at) an L1 Halo orbit triple cover at $C = 2.998$ after going through many bifurcations. As for the remaining 4 bifurcating spatial families, we did not find any natural ending or interesting connections, at least within the extent of our continuations.

Planar symmetry-breaking bifurcations Changes of planar CZ indices alerted us to 7 planar orbit bifurcations, which were again confirmed by computing planar Floquet multipliers. Of these, 3 are fold bifurcations where C takes an extremum, as shown in dark blue in Fig. 5; the remaining 4 are symmetry-breaking bifurcations and are shown in orange in the same figure. These are the only two possible planar bifurcation types for symmetric planar CR3BP orbits;[17] the latter generates new, asymmetric orbit family pairs.

Of the 4 symmetry-breaking bifurcations shown, the most interesting are those in the H1 orbits at $C = 2.489$ and -0.735. These are in fact connected by the resulting asymmetric orbit family pair. The relation of this asymmetric planar PO family to H1 is shown in Figure 8, along with plots of a few family POs; the second asymmetric family will have orbits that are the y-axis reflections of those shown. This family passes through the singularity at Earth twice, and has a bifurcation of its own at $C = -0.855$ from which new orbits

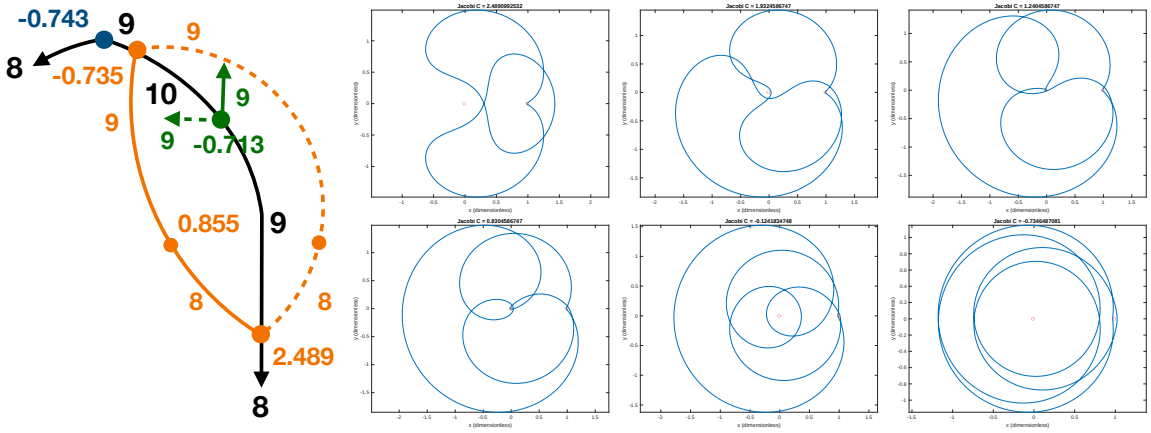

Figure 8: Bifurcation graph & orbits for asymmetric planar family emerging from H1, with CZ indices & bifurcation C values labeled. Dotted lines indicate family obtained by reflection. Orbits on right are ordered by decreasing C moving right and down, start/end at critical symmetric H1 orbits

should emerge, though we did not investigate these further. Of the other two symmetry-breaking bifurcations, we found the asymmetric family pair emerging from H2 at $C = 2.270$ (not shown) ends at a planar symmetric PO of unknown type. We have not yet found an end for the orbit family pair emerging from $C = -1.084$.

Earth Prograde Orbits, the 2:1 Mean Motion Resonance, and Bifurcations

We next study the PO family which starts as small prograde circles around Earth. These were also studied by Broucke,[1] who called this the BD family. It turns out that most BD orbits are in 2:1 mean motion resonance with the Moon: the spacecraft makes approximately 2 revolutions around the Earth in the time the Moon makes one. As detailed in Kumar et al,[18] the BD family starts out as prograde non-resonant circles, which then morph into prograde stable 2:1 resonant orbits. These pass through the singularity at Earth and become retrograde 2:1 stable, then undergo a fold bifurcation at $C = 0.0604$ and become retrograde 2:1 unstable, and then again pass through the Earth singularity and become prograde 2:1 unstable. These last orbits then encounter another fold at $C = 3.152$, after which the orbits very briefly become stable, followed by a planar symmetry-breaking bifurcation and instability again. The orbits leave the 2:1 resonance soon after this fold.

Our investigation of this family did not continue the orbits beyond those of Broucke's 1968 report; instead, we focus on the bifurcation analysis of the BD family, for which a diagram is shown in Figure 9. The previously-mentioned fold and planar symmetry-breaking bifurcations are clearly visible on the diagram, as well as several out-of-plane bifurcations which lead to new spatial PO families. Again, we analyzed every single BD family bifurcation up to the non-2:1 resonant unstable BD orbit at $C = 3.10$; thus, all bifurcations of the 2:1 resonant BD orbits are accounted for. The Floer numbers before and after each BD bifurcation point can again be verified to match, indicating all orbits emerging from those points have been found.

Out-of-plane bifurcations As shown in Figure 9, there are four out-of-plane bifurcations in the studied portion of the BD family. The ones at $C = 2.762$ and 2.537 occur in the stable prograde 2:1 part of BD, while those at $C = 3.148$ and 3.143 occur near the end of the unstable prograde 2:1 orbits of BD. The retrograde portions of BD display no single-cover bifurcations of any kind. Bifurcation diagrams summarizing details of the two sets of spatial bifurcations (as well as the one planar bifurcation) are shown in Figure 10.

Looking first at the stable orbits' bifurcations, the spatial bifurcation at $C = 2.762$ creates an xz-symmetric orbit family pair connecting a prograde 2:1 BD orbit to vertical Earth-collision orbits, indicated by green x's in the diagram. The spatial bifurcation at $C = 2.537$ also starts at a stable prograde 2:1 orbit, but the resulting axially-symmetric orbit family pair ends at a triple cover of a planar Earth retrograde orbit, at $C = 0.0080$ (Earth retrograde orbits will be discussed in the next section). Fig. 11 shows a few orbits from this prograde-to-retrograde family; they are all very mildly unstable and could be suitable as long-term spacecraft orbits.

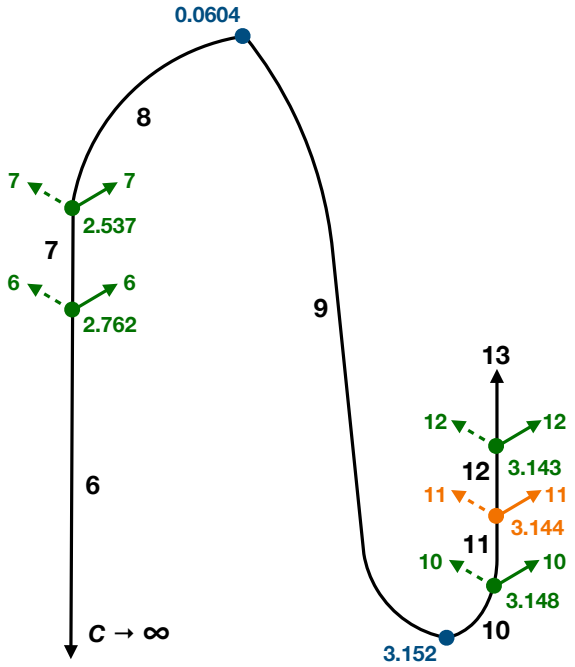

Figure 9: Bifurcation diagram for the BD Earth prograde family. Same color coding and labels as Fig. 5

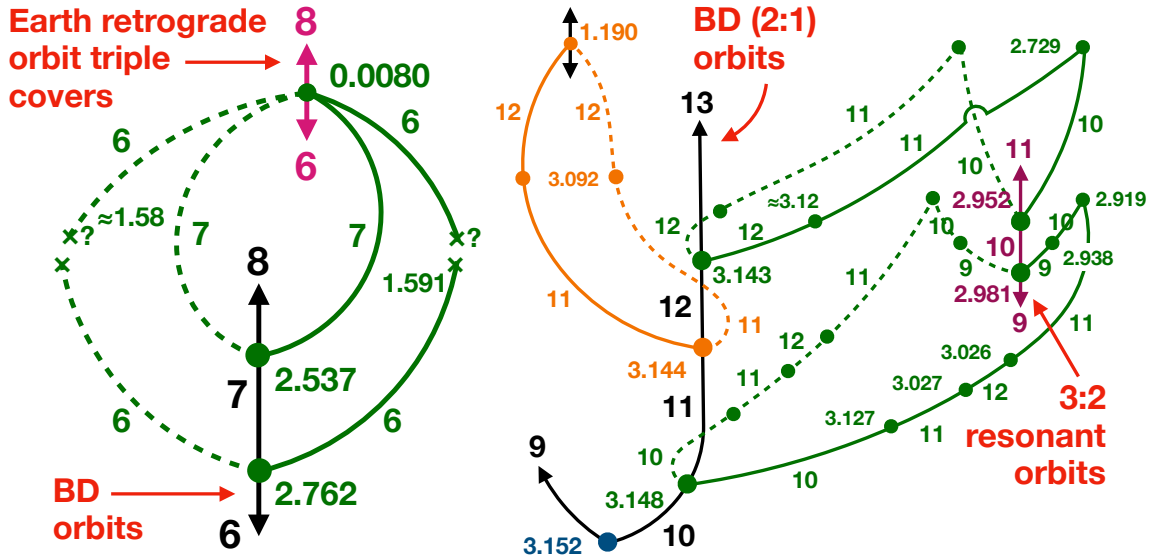

Figure 10: Bifurcation diagrams for (L) stable prograde 2:1 BD orbit spatial bifurcations to Earth retrograde & vertical collision orbits, x marks collision; (R) various bifurcations after the $C = 3.152$ fold bifurcation

The other two out-of-plane bifurcations from BD occur among its last unstable 2:1 resonant orbits, at $C = 3.148$ and 3.143. Both bifurcations create spatial families which end at planar symmetric 3:2 resonant orbits, suggesting that spatial orbit families may create links between planar periodic orbits at *different* resonances. The xz-symmetric family emerging at $C = 3.148$ is shown in Figure 12. the third orbit in the top row of Fig. 12 seems to have a "loop" near the Moon that resembles a Halo orbit, suggesting that such orbits may be useful for transfers from the 2:1 resonance to Halo orbits. Most orbits in this family are moderately unstable, with some regions of stability as well; indeed, the family undergoes several additional spatial-to-spatial orbit bifurcations as well, marked in Fig. 10 but not investigated further. The orbit family emerging at $C = 3.143$ (not pictured) has axial symmetry; it displays mild to moderately instability throughout the entire family.

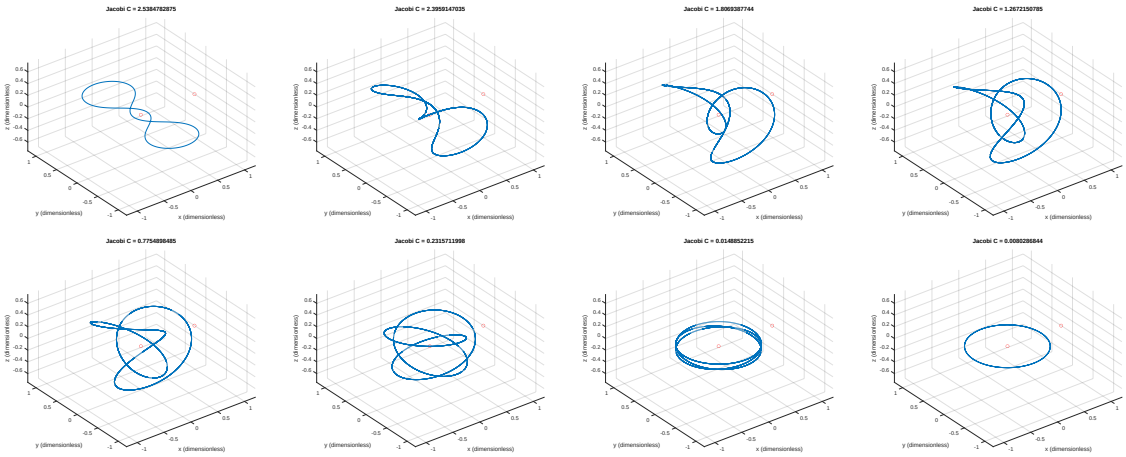

Figure 11: Spatial orbits from the BD stable prograde 2:1 to Earth retrograde triple-cover orbit family

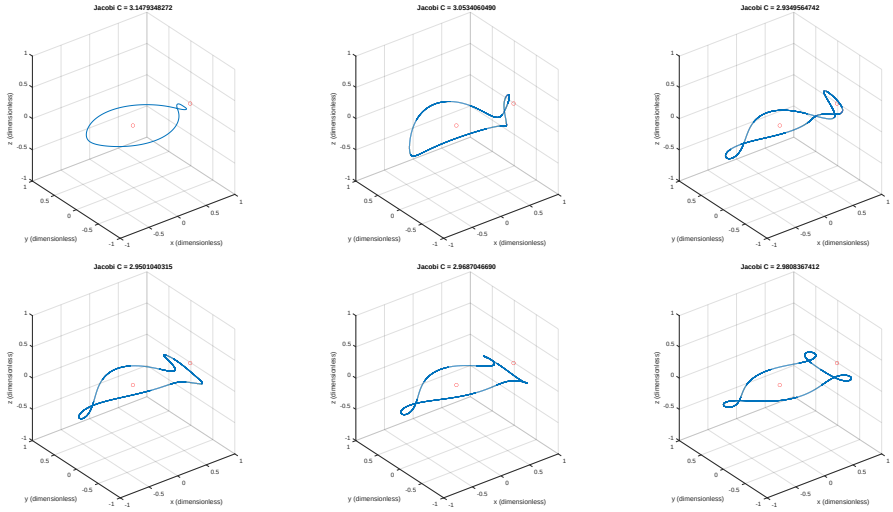

Figure 12: Spatial orbits from the BD stable prograde 2:1 resonant to a 3:2 resonant planar orbit family

Planar symmetry-breaking bifurcations The BD orbits studied only encounter one planar symmetry-breaking bifurcation, at one of the final 2:1 resonant prograde unstable BD orbits at $C = 3.144$, as shown on the right diagram of Figure 10. An asymmetric orbit family pair emerges there, ending at $C = 1.190$ at a planar symmetric orbit of unknown type (we did not compute more of this symmetric family or its CZ indices). The orbits are displayed in Figure 13. Parts of several orbits' shapes visually resemble "rotated" versions of various symmetric BD 2:1 resonant orbits; an investigation of these orbits' relationship with regions of librational 2:1 resonant tori (see e.g. Rawat et al[19]) could help shed light on the underlying causes of this observation. Most of this family is quite unstable, which could facilitate useful resonance-to-resonance heteroclinic transfers similar to those found to/from symmetric BD 2:1 orbits in Kumar et al.[18]

Lunar and Earth Retrograde Orbits and Infinite Chains of Resonant Orbits

With both lunar and Earth prograde orbits thoroughly studied, we turn our attention to PO families that start as small retrograde orbits around the Earth or Moon. Once again, Broucke studied these families in his 1968 report,[1] labeling the families generated by Earth and Moon retrograde orbits as A1 and C respectively. The lunar retrograde family C includes what are also now known as the distant retrograde orbits (DROs). Both families A1 and C encounter collisions with the Earth and Moon. Broucke noted that these collisions generate loops around the Earth or Moon, and computed two A1- and one C-family collision orbit. However, he did not go further, remarking that "the natural end of the family has not yet been determined".

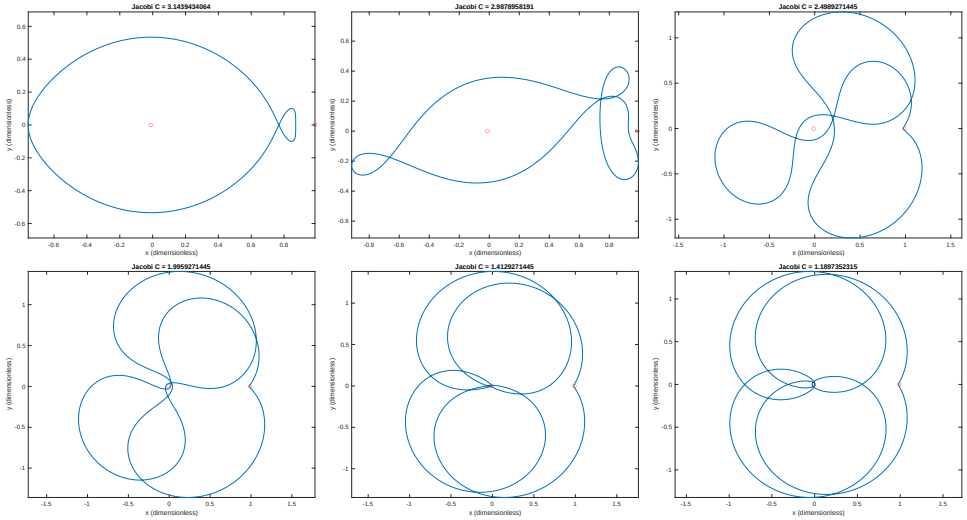

Figure 13: Planar asymmetric orbits emerging from BD unstable prograde orbit, ending in symmetric orbit

Again leveraging our KS-regularized symmetric orbit continuation method to continue A1 and C beyond Broucke's last orbits, we have discovered a remarkable pattern followed by both orbit families, strongly suggesting that these families grow ad-infinitum with no "natural end" to be found. In short, after its first collision with the Moon, the Earth-centered retrograde family A1 extends to a (seemingly infinite) chain of $1{:}2N$ exterior resonant periodic orbits, $N \in \mathbb{Z}^+$. Similarly, the lunar retrograde C family extends to a chain of $1{:}2N+1$ exterior resonant periodic orbits after its first lunar collision. Figure 14 displays a selection from the extended A1 family showing its evolution from Earth retrograde to 1:2, then 1:4, and finally 1:6 resonant orbits; Figure 15 displays the evolution of the extended C family from lunar retrograde to 1:3, 1:5, and 1:7. Though not shown in these plots, we verified this pattern up to 1:12 resonance for A1 and up to 1:11 for C.

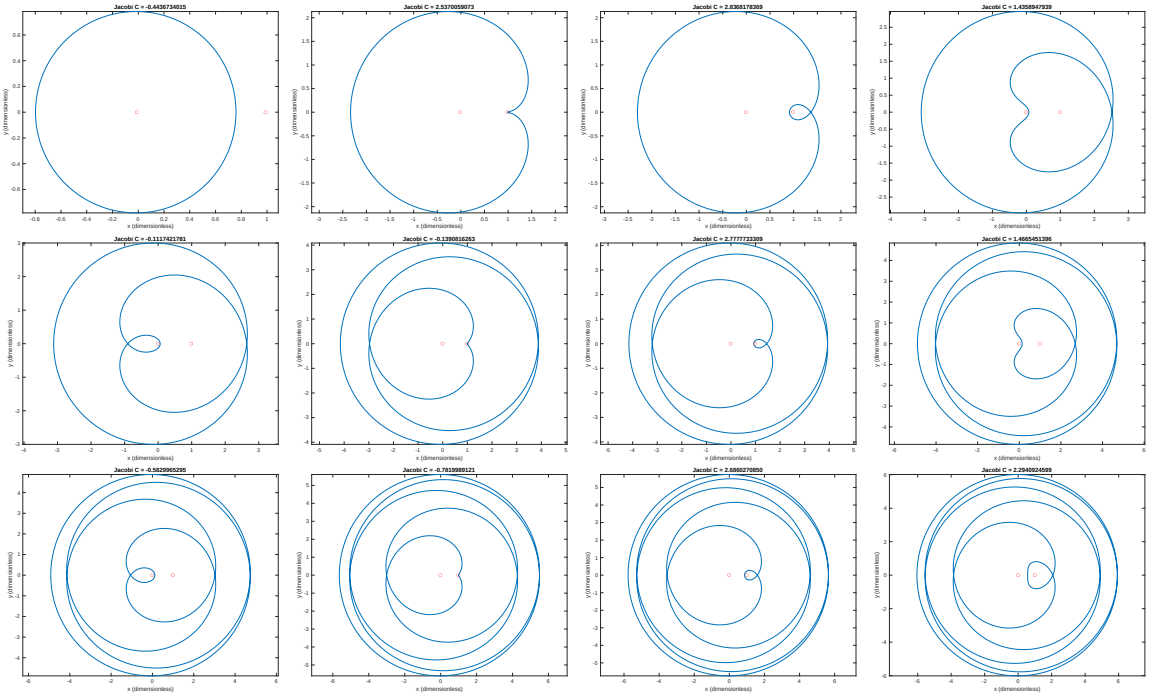

Figure 14: Evolution of Earth retrograde A1 family, with Earth collision and Moon collision-induced loop-spawning and resonance changes chaining Earth retrograde, 1:2, 1:4, 1:6, ... orbits together.

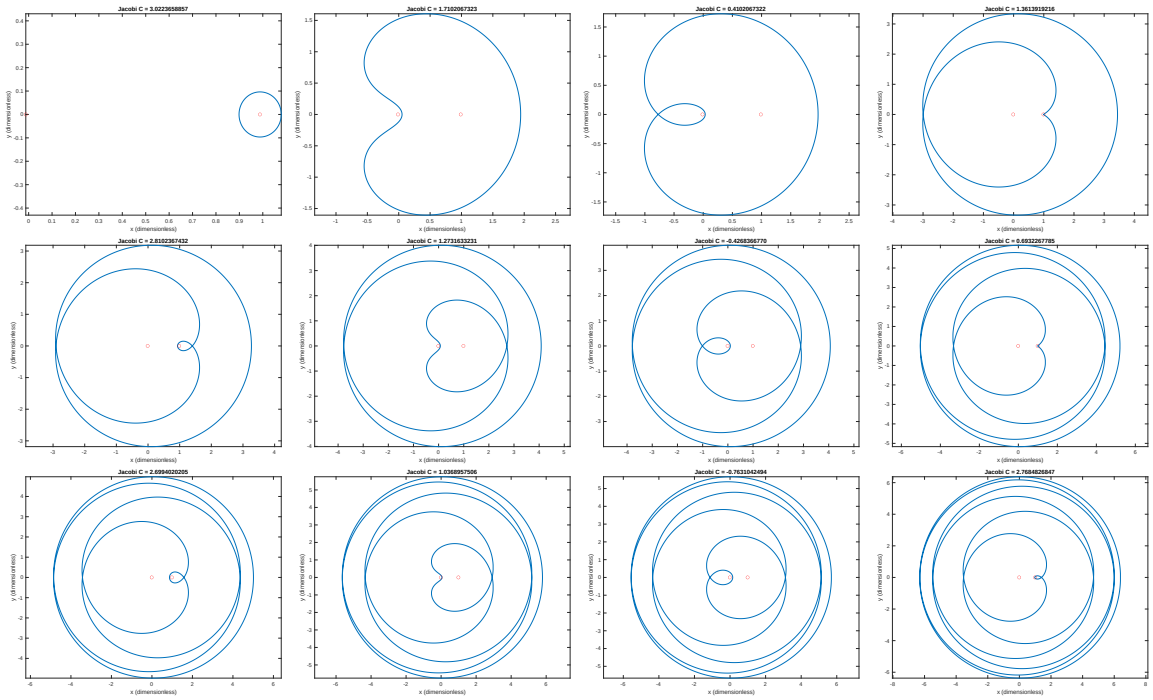

Figure 15: Evolution of lunar retrograde C family, with Earth collision and Moon collision-induced loop-spawning and resonance changes chaining lunar retrograde, 1:3, 1:5, 1:7, ... orbits together.

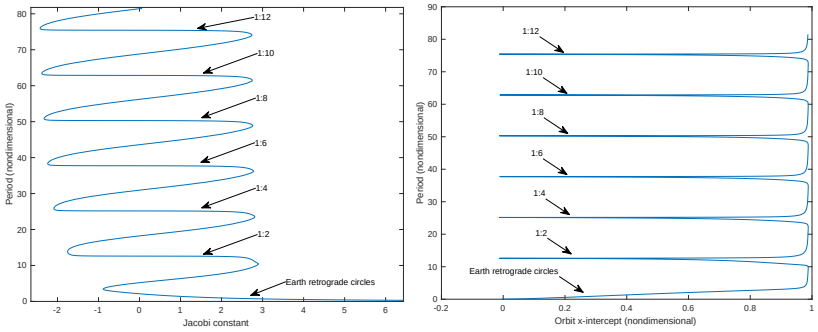

Figure 16: (L) A plot of orbit period vs Jacobi constant along the A1 orbit family chain of 1:2N resonant orbits, with resonances labeled. (R) A plot of orbit period vs orbit x-intercept along the same chain,

Figures 14 and 15 illustrate the mechanism by which the orbits spawn increasing numbers of "loops" corresponding to changes between prograde to retrograde motion and changes of resonance ratio. For the A1 example, we start with a non-resonant circular retrograde Earth orbit on the top left of Figure 14. Then, moving right and down the figure plots, we get 2) the retrograde circle approaching the Moon, 3) a prograde 1:2 resonant orbit with a new loop after passing through the Moon, 4) a prograde 1:2 orbit with the loop having grown, nearing Earth collision, 5) a 1:2 orbit that has become retrograde, with another new loop, after having passed through Earth, and 6) the 1:2 orbit with a grown loop nearing Moon collision. Plots 7-12 show this process of Moon and then Earth collisions continuing with 1:4 orbits (7-10) and finally ending at 1:6 orbits (11-12). This seems to continue ad infinitum, chaining the 1:2N orbits together. The C family of Figure 15 behaves very similarly, with 1) a retrograde moon orbit morphing into 2) an Earth prograde orbit, which 3) passes through the Earth singularity and becomes Earth 1:1 resonant retrograde, followed by a similar loop growth-Moon collision-loop growth-Earth collision 1:2$N+1$ orbit chain as in A1.

Plotting the orbit period vs Jacobi constant and x-intercept along A1 and C in Figures 16 and 17, respectively, one clearly sees jumps in orbit period to the next resonance (e.g. 1:2 to 1:4, 1:3 to 1:5, etc) every time the family passes near and then through the Moon singularity at $x = 1 - \mu$. From the right plots of both

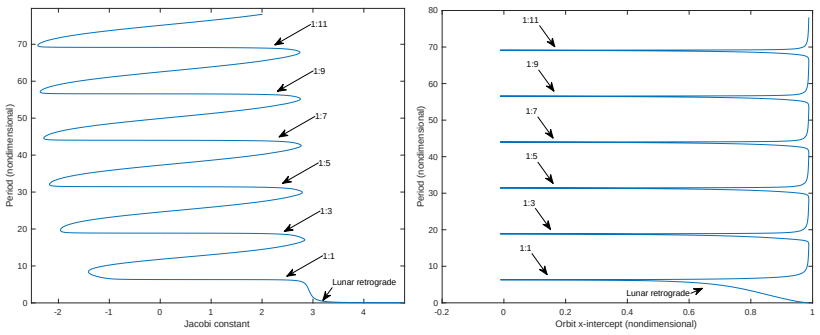

Figure 17: (L) A plot of orbit period vs Jacobi constant along the C orbit family chain of $1{:}2N-1$ resonant orbits, with resonances labeled. (R) A plot of orbit period vs orbit x-intercept along the same chain,

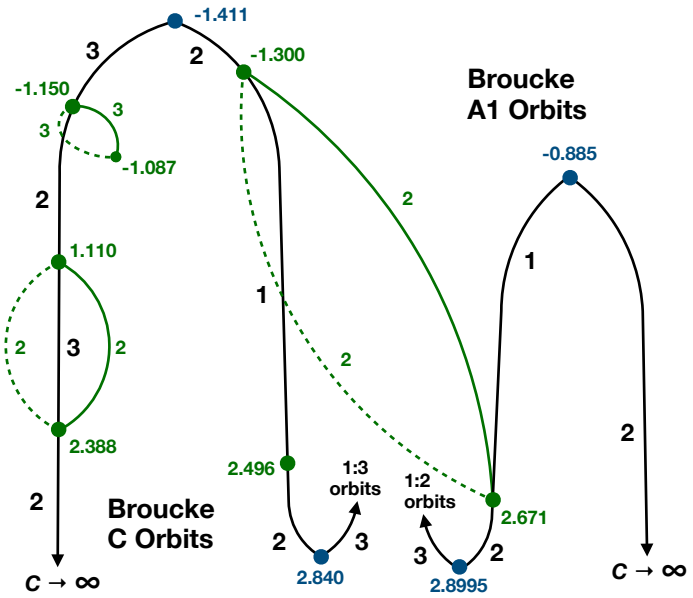

Figure 18: Bifurcation diagram for Broucke's A1 and C families, which are generated by small circular Earth and lunar retrograde orbits respectively. Same color coding and labels as Fig. 5

figures, note that the physical extent (in x, y, z space) of the orbits where the period and Jacobi constant increase dramatically is actually quite small compared to the orbit families themselves. Given the fundamental role of the lunar singularity in chaining these orbits together, the KS regularized orbit continuation methods were crucial in uncovering this familial relationship between seemingly unrelated resonant orbits.

Bifurcations With the Earth & Moon retrograde-orbit-generated families A1 and C characterized, we next studied their bifurcations. Given these PO families' presumed infinite nature, we only studied bifurcations of the A1 & C orbits between the families' origins as small retrograde circles, and their Moon collision-induced transitions to 1:2 and 1:3 resonances, respectively. The resulting diagram is shown in Figure 18. As is clearly visible, there are significantly fewer bifurcations of the studied A1 and C orbit single covers than the prograde orbit case, with only 5 spatial bifurcations in the C family and one in A1; all were studied except the one at $C = 2.496$, as it is very close to collision. No planar bifurcations (apart from folds) were found.

Of the 5 spatial C family bifurcations, the two at $C = 2.388$ and 1.110 are joined by the same spatial family pair; its orbits have fairly low out-of-plane amplitude and closely mirror the shape of planar C family DRO and Earth prograde orbits. The bifurcation at $C = -1.150$ produces the very mildly unstable spatial family shown in Figure 19; the last orbit shown is approximately the xy-plane reflection of the second, and connects back to the first one when continued further. Finally, from the bifurcation at $C = -1.300$ (a retrograde geocentric C family orbit) emerges a spatial family – shown in Fig. 20 – connecting this C orbit to a near

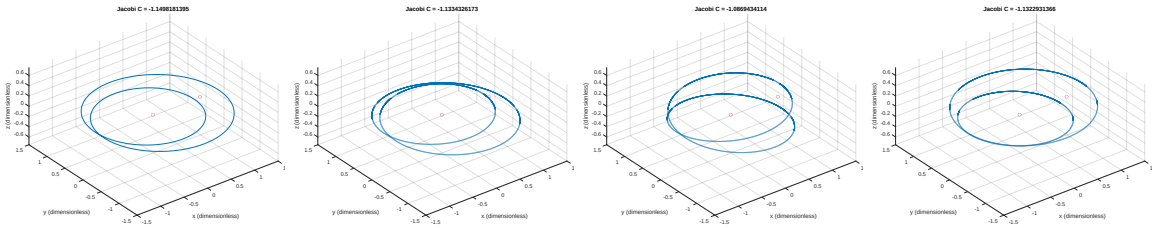

Figure 19: Spatial orbits emerging from C family bifurcation at $C = -1.150$

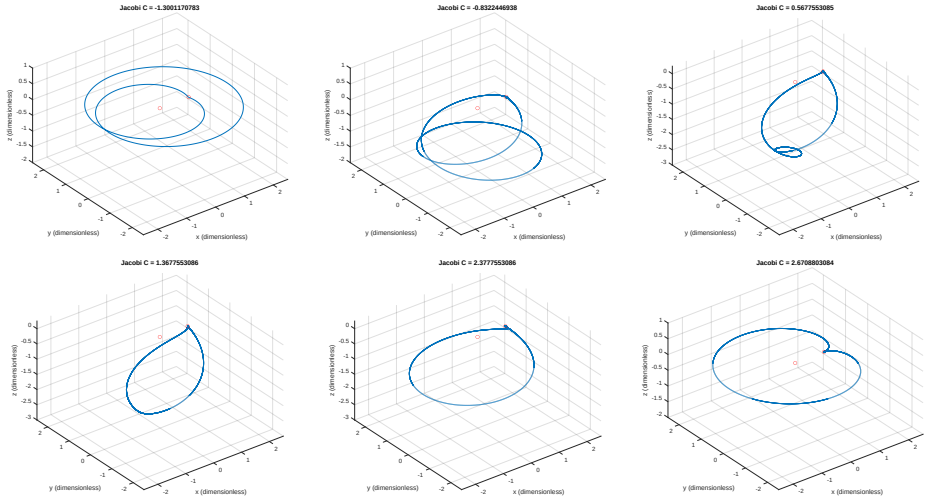

Figure 20: Spatial orbits connecting C family retrograde orbit to A1 family orbit

Moon-collision retrograde A1 orbit. These orbits are highly unstable, as all make close flybys of the Moon.

CONCLUSION

In this paper, we leveraged numerical continuation, Kustaanheimo-Stiefel regularization, and tools from modern symplectic geometry to conduct a thorough bifurcation analysis of singly-covered CR3BP periodic orbit families generated by Earth & Moon prograde & retrograde orbits. The use of CZ indices and Floer invariants, facilitated by our new publicly available MATLAB program, provided very simple ways of detecting bifurcations and validating our analyses thereof. Our KS regularization-enabled orbit computation methods proved crucial, allowing for orbit continuation through singularities where past studies usually stop.

Combining these tools and methods, we found new periodic orbit families, uncovered previously-unknown connections between them, and revealed the network structure of these families across a number of Earth-Moon orbital regimes. We positively confirmed a 1968 conjecture of R. Broucke, discovered "chains" unifying periodic orbits across various resonances into just two orbit families, and computed many other orbits. Spatial orbit families were found that form geometric "bridges" connecting planar DPOs/LPOs with Halos, lunar LPO with DPO, and Earth planar prograde with retrograde orbits, among many others.

While many of the orbits found are too unstable or near-collision for applications – being instead of more academic interest – others are of potential practical use. For example, the LPO-Halo bridges of Fig. 6 include moderately unstable orbits whose manifolds could yield transfers to the vicinity of stable Halo orbits. The family of Fig. 12 has both stable & unstable orbits which make Halo-like lunar excursions and then come back near Earth - thus being potentially useful for cislunar PNT spacecraft or even transfers. The orbits of Fig. 13 seem to be related to the 2:1 resonance, which should be investigated further. Future research should also look at period-doubling & n-fold bifurcations of the PO families whose single covers were studied here.

One key takeaway from this paper should be the importance of regularization for computing previously-unknown orbits. Another should be how one can now very easily leverage symplectic tools to aid in PO

bifurcation analysis. And finally, in general we hope that this understanding of the network structure of PO families will provide a useful way of organizing information on these orbits, in a way that large databases do not. For example, a mission planner seeking orbits similar to Halo or LPO orbits may find orbits from nearby bifurcating families useful as well, for which the diagram of Fig. 6 could be helpful. The network diagram of Doedel et al[3] on PO families near L1-L5 is often referred to by astrodynamicists, and we hope that this study may serve as a stepping stone towards similar understanding in other cislunar regimes as well.

Acknowledgments

B. Kumar was supported by the US Air Force Office of Scientific Research (AFOSR) under Award No. FA8655-24-1-7012 and by the National Science Foundation under Award no. DMS-2202994. A. Moreno is currently supported by the Sonderforschungsbereich TRR 191 Symplectic Structures in Geometry, Algebra and Dynamics, funded by the DFG (Projektnummer 281071066 – TRR 191) under Germany's Excellence Strategy EXC 2181/1 - 390900948 (the Heidelberg STRUCTURES Excellence Cluster), and by the AFOSR under Award No. FA8655-24-1-7012.

REFERENCES

[1] R. Broucke, "Periodic Orbits in the Restricted Three-Body Problem with Earth-Moon Masses," Tech. Rep. No. 32, Jet Propulsion Laboratory, Pasadena, CA, 1968.

[2] K. C. Howell and J. V. Breakwell, "Almost rectilinear halo orbits," *Celestial mechanics*, Vol. 32, No. 1, 1984, pp. 29–52, 10.1007/BF01358402.

[3] E. J. Doedel, V. A. Romanov, R. C. Paffenroth, H. B. Keller, D. J. Dichmann, J. GalÁN-Vioque, and A. Vanderbauwhede, "Elemental Periodic Orbits Associated With the Libration Points in the Circular Restricted 3-Body Problem," *Int. J. Bifurc. Chaos.*, Vol. 17, No. 08, 2007, pp. 2625–2677.

[4] C. J. Franz and R. P. Russell, "Database of Planar and Three-Dimensional Periodic Orbits and Families Near the Moon," *J. Astronaut. Sci.*, Vol. 69, No. 6, 2022, pp. 1573–1612, 10.1007/s40295-022-00361-9.

[5] U. Frauenfelder, D. Koh, and A. Moreno, "Symplectic methods in the numerical search of orbits in real-life planetary systems," *SIAM J. Appl. Dyn. Syst.*, Vol. 22, No. 4, 2023, pp. 3284–3319.

[6] P. Kustaanheimo, A. SCHINZEL, H. DAVENPORT, and E. STIEFEL, "Perturbation theory of Kepler motion based on spinor regularization.," *Journal für die reine und angewandte Mathematik*, Vol. 1965, No. 218, 1965, pp. 204–219, doi:10.1515/crll.1965.218.204.

[7] A. E. Roy and M. W. Ovenden, "On the Occurrence of Commensurable Mean Motions in the Solar System: The Mirror Theorem," *Mon. Not. R. Astron. Soc.*, Vol. 115, 06 1955, pp. 296–309.

[8] I. A. Robin and V. V. Markellos, "Numerical determination of three-dimensional periodic orbits generated from vertical self-resonant satellite orbits," *Celestial mechanics*, Vol. 21, No. 4, 1980, pp. 395–434.

[9] A. Moreno, C. Aydin, O. v. Koert, U. Frauenfelder, and D. Koh, "Bifurcation Graphs for the CR3BP via Symplectic Methods," *J. Astronaut. Sci.*, Vol. 71, No. 6, 2024, p. 51.

[10] U. Frauenfelder and A. Moreno, "On GIT quotients of the symplectic group, stability and bifurcations of periodic orbits (with a view towards practical applications)," *J. Symplectic Geom.*, Vol. 21, No. 4, 2023, pp. 723–773, 10.4310/jsg.2023.v21.n4.a3.

[11] R. Broucke, "Stability of periodic orbits in the elliptic, restricted three-body problem.," *AIAA J.*, Vol. 7, 1003, 1969.

[12] C. Conley and E. Zehnder, "Morse-type index theory for flows and periodic solutions for Hamiltonian equations," *Comm. Pure Appl. Math.*, Vol. 37, No. 2, 1984, pp. 207–253, 10.1002/cpa.3160370204.

[13] J. Robbin and D. Salamon, "The Maslov index for paths," *Topology*, Vol. 32, No. 4, 1993, pp. 827–844.

[14] M. Lara and R. P. Russell, "On the family 'g' of the restricted three-body problem," *Monografias de la Real Academia de Ciencias de Zaragoza*, Vol. 30, 2006, pp. 51–66.

[15] C. Aydin and A. Batkhin, "Studying network of symmetric periodic orbit families of the Hill problem via symplectic invariants," *Celest. Mech. Dyn. Astron.*, Vol. 137, No. 2, 2025, p. 12.

[16] K. Howell and E. Campbell, "Three-dimensional periodic solutions that bifurcate from halo families in the circular restricted three-body problem," *Adv. Astronaut. Sci.*, Vol. 102, 01 1999, pp. 891–910.

[17] R. Rimmer, "Symmetry and bifurcation of fixed points of area preserving maps," *Journal of Differential Equations*, Vol. 29, No. 3, 1978, pp. 329–344, https://doi.org/10.1016/0022-0396(78)90044-X.

[18] B. Kumar, A. Rawat, A. J. Rosengren, and S. D. Ross, "Investigation of Interior Mean Motion Resonances and Heteroclinic Connections in the Earth-Moon System," *75th International Astronautical Congress*, Milan, Italy, 2024.

[19] A. Rawat, B. Kumar, A. J. Rosengren, and S. D. Ross, "Cislunar Mean-Motion Resonances: Definitions, Widths, and Comparisons with Resonant Satellites," 2025.